THE JOURNAL OF PHYSICAL CHEMISTRY C

Article

Cite This: J. Phys. Chem. C 2019, 123, 22711−22724

pubs.acs.org/JPCC

Evaporation vs Solution Sequential Doping of Conjugated Polymers: F_4TCNQ Doping of Micrometer-Thick P3HT Films for Thermoelectrics

Matthew T. Fontana,[†,‡] Dane A. Stanfield,[†,‡] D. Tyler Scholes,[†] K. J. Winchell,[†] Sarah H. Tolbert,[*,†,§] and Benjamin J. Schwartz[*,†]

[†]Department of Chemistry and Biochemistry, University of California, Los Angeles, Los Angeles, California 90095-1569, United States

[§]Department of Materials Science and Engineering, University of California, Los Angeles, Los Angeles, California 90095-1595, United States

Supporting Information

ABSTRACT: For thermoelectric and other device applications there has been great interest in the chemical doping of conjugated polymer films. Solution doping followed by film deposition generally produces poor-quality films, but this issue can be alleviated by sequential doping: a pure polymer film is deposited first, and the dopant is then added as a second processing step, preserving the quality and structure of the original polymer film. In this paper, we compare two methods for sequential doping of conjugated polymer films: evaporation doping, where a controlled thickness of dopant is added via thermal sublimation to a temperature-controlled polymer film, and sequential solution doping, where the dopant is spin cast from a solvent chosen to swell but not dissolve the underlying polymer film. To compare these two different types of sequential doping, we examine the optical, electrical, and structural properties of poly(3-hexylthiophene-2,5-diyl) (P3HT) films doped by each method with the small-molecule dopant 2,3,5,6-tetrafluoro-7,7,8,8-tetracyanoquinodimethane (F_4TCNQ) as a function of the polymer film thickness. Although each method intercalates dopant in fundamentally unique ways, we find that both vapor and solution doping methods produce films that share many of the same properties. Interestingly, both methods can produce doped P3HT films with conductivities of ∼5 S/cm and comparable thermoelectric properties, even for films as thick as 400 nm. For the evaporation method, an "overhead" dopant film thickness of ∼6 nm is required, either to promote reorganization of existing crystallites or to fill preexisting trap states in the polymer film. After the overhead amount has been deposited, the thickness of the dopant layer that must be evaporated to reach the optimal electrical conductivity is ∼1/3 that of the underlying polymer film. For a given P3HT film thickness, the amount of evaporated dopant needed to produce the highest conductivity corresponds to a thiophene monomer to ionized dopant ratio of ∼8.5:1. For solution processing, with the appropriate choice of solvent and dopant concentration, we show that P3HT films as thick as 2 μm can be doped to achieve conductivities of ∼5 S/cm and thermoelectric power factors approaching 2 $\mu W/mK^2$. For either method, if excess dopant is applied, it remains in neutral form either in the amorphous regions or on top of the film, reducing the conductivity by increasing the film thickness. For both methods, UV−vis absorption can be used as a quick proxy to easily monitor whether saturation doping levels have been reached or exceeded. Fourier transform infrared spectroscopy (FTIR) and grazing-incidence wide-angle X-ray scattering (GIWAXS) both show that vapor-doped films and thicker solution-doped films have improved morphologies that result in more mobile carriers. Overall, we demonstrate that it is a straightforward process to select a sequential doping method for a desired application: evaporation doping is more amenable to large-area films, while solution doping is lower cost and better suited for polymer films with micrometer thicknesses.

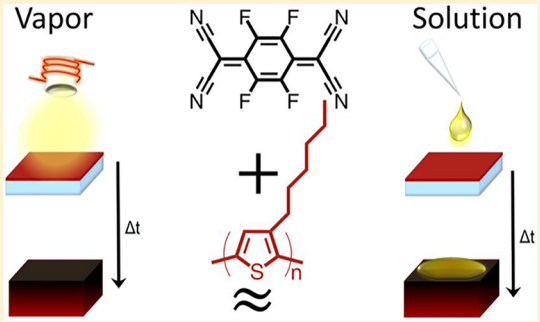

1. INTRODUCTION

Conjugated polymers are of considerable interest since they are semiconducting[1−3] and low cost,[4,5] have mechanical flexibility,[6,7] are easily solution processed,[4,8] and have properties that are readily tuned synthetically.[4,9] As a result, these materials are ideally suited for a wide variety of device applications.[10−13]

As with inorganic semiconductors, it is possible to dope conjugated polymers to increase their equilibrium carrier density and thus modify their electrical properties. Unlike inorganic semiconductors, which are doped by atomic substitution, organic semiconductors are usually doped chemically by adding a strong oxidizing (or reducing) agent. When doped, semiconducting polymers show particular promise as active materials for thermoelectrics[1,14−20] due to their reasonably high electrical conductivities and generally

Received: May 28, 2019
Revised: August 2, 2019
Published: August 20, 2019

DOI: 10.1021/acs.jpcc.9b05069
J. Phys. Chem. C 2019, 123, 22711−22724

poor thermal conductivities.[14,17,21,22] This explains the recent surge of research on the multiple ways to produce molecularly doped conjugated polymers; this research includes studies on the methodologies used to produce doped polymer films as well as studies on the performance of devices fabricated from such materials.[23−30]

It is well established that the electrical conductivity of semiconducting polymers can be effectively tuned over several orders of magnitude by changing the amount of dopant used.[27,31−33] What is less clear, however, is the maximum possible degree of doping that can be achieved. Part of the reason for this is that there are multiple different methods for producing doped polymer films. The most common method involves casting a film of pre-doped polymer created by blending the polymer and dopant in solution, which we refer to as blend-cast doping.[15,19,22,23,26,33−35] This method makes it difficult to produce high doping levels, however, because as conjugated polymers become charged in solution they generally become much less soluble, making it difficult to cast high-quality films.[15,23,36−39] Because of this there has been a great deal of recent effort aimed at starting with undoped conjugated polymer films and then exposing the pre-cast films to the dopant in a secondary step.

Different groups implemented this latter approach, which we term sequential doping, in various ways. Some researchers expose the polymer film to the dopant molecules in the vapor phase,[33,40,40−43] as outlined schematically in Figure 1a.

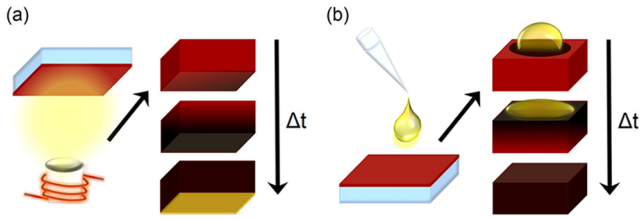

Figure 1. Schematic showing sequential doping of conjugated polymer films using (a) evaporation sequential doping and (b) solution sequential doping; after the initial step, the arrows in each panel indicate the changes that take place as a function of time. (a) For evaporation doping the crucible is resistively heated, producing dopant vapor (yellow) that can intercalate into a pre-cast polymer film (red). With additional time a greater amount of dopant intercalates within the polymer film (doped film is indicated with black color). If evaporation continues, the dopant is added in excess, eventually coating the exposed side of the film. (b) For solution doping a dopant solution (yellow) is spin cast onto a pre-cast polymer film (red). Solvent for the dopant solution is chosen to swell but not dissolve the polymer, allowing mass action to drive the dopant from the solution into the swollen film. Films can be more strongly doped (increasing black color) by increasing the concentration of the dopant in solution.

Alternatively, some groups, including ours, pursued a solution-based technique where the dopant is directly spin coated from solution onto a pre-cast polymer film,[18,23−26,44,45] represented in Figure 1b. The purpose of this paper is to compare in detail the evaporation and solution-based sequential doping methods to determine which method, if either, is better for particular applications, such as thermoelectrics. This is accomplished through a head-to-head comparison of the films' optical, electrical, and structural properties. To our knowledge, this is the first study performed to date that compares the two doping methods side-by-side on identical pre-cast polymer films. Furthermore, our comparison extends to films that are hundreds of nanometers thick, a thickness regime that is largely uncharacterized in the literature.

Evaporation sequential doping has been the subject of many recent reports, most of which have focused on the doping of poly(3-hexylthiophene-2,5-diyl) (P3HT) by 2,3,5,6-tetrafluoro-7,7,8,8-tetracyanoquinodimethane (F_4TCNQ).[33,42] These reports attributed the high electrical conductivities observed after doping to the idea that the crystalline order of the pre-cast polymer films is preserved after doping. Similar conclusions have been reached upon evaporation doping of poly(2,5-bis(3-alkylthiophen-2-yl)thieno[3,2-*b*]thiophene) (PBTTT).[46] Although evaporation sequential doping yields high conductivities, most reports focus on films that are only a few tens of nanometers thick.[40−42,46]

Another open question with evaporation doping is how to reproducibly control the amount of dopant delivered. This is because most experimental evaporation doping setups add the dopant by sublimation in a home-built chamber with no way to precisely monitor the amount of dopant deposited on the polymer film.[33,41−43] An additional issue is the fact that the sublimation process tends to heat polymer films: heating promotes increased diffusion of dopant species, and heating-induced diffusion may vary among different polymer/dopant systems. This leads to potential difficulties with reproducibility if the temperature of the film cannot be precisely controlled.[41,42] Very few studies have focused on more quantitative methods for delivering a precise amount of dopant, such as using a thermal evaporator with thickness monitoring.[40]

Solution sequential doping has also been the focus of much recent work.[18,19,23−26,43−45,47,48] Methods for solution sequential doping include (1) immersing the film in a dopant solution, (2) drop casting the dopant solution onto the polymer film, and (3) spin coating the dopant solution onto the polymer film. Although film immersion and drop casting can effectively dope polymer films, we focus here on doping by spin coating due to its facility in producing high-quality films.[23−25] With spin coating, the dopant is dissolved in a solvent that is chosen to optimally swell but not dissolve the polymer of interest. When the dopant solution is spin coated onto a pre-cast polymer film, mass action drives the dopant from the solution into the swollen polymer underlayer.[23−26,49−51] As with evaporation doping, solution sequential doping maintains much of the pre-cast polymer film's morphology, leading to excellent film quality and high electrical conductivities.[23−26] Moreover, because the method involves the spin coating of a dopant solution with a precisely defined concentration, the reproducibility of the method is high.[23−26,44]

Solution sequential processing is limited, however, by the need to find solvents that simultaneously dissolve the dopant and optimally swell the polymer but do not dissolve the polymer underlayer. Since it is generally straightforward using solvents or solvent blends to optimally swell a conjugated polymer film,[26,50] the limiting factor for dopant intercalation with solution sequential doping is usually the solubility of the dopant in the selected swelling solvent.[52]

Despite the widespread and increasing application of sequential doping via evaporation and solution processing, no head-to-head comparison between the two methods has been carried out. In this work, we consider the similarities and differences between the evaporation and the solution

DOI: 10.1021/acs.jpcc.9b05069
J. Phys. Chem. C 2019, 123, 22711−22724

sequential doping methods, focusing on the well-studied P3HT/F_4TCNQ materials combination. Of particular interest is the way each method scales for doping conjugated polymer films of increasing thicknesses. For our evaporation-sequential-doping experiments, we employ a thermal evaporator to intercalate the F_4TCNQ dopant into films of P3HT. The films are actively held at a fixed temperature, and the extent of deposition is calibrated using a quartz crystal microbalance (QCM) thickness monitor, providing quantitative and reproducible dopant delivery. Our solution sequential doping measurements rely on spinning F_4TCNQ from dichloromethane (DCM), which is a near-optimal solvent for swelling P3HT.[23−26,50,51,53,54] Since both techniques are sequential, we are able to make detailed comparisons between the two methods by doping identical pre-cast films of P3HT.

Using these two methods we find that the electrical conductivities and thermoelectric performance of doped films are comparable if each method is properly applied. For evaporation doping, after an "overhead" thickness of ∼6 nm of F_4TNCQ is deposited, the optimal degree of doping is achieved when a thickness ratio of ∼1:3 dopant:polymer is reached, corresponding to a thiophene monomer:ionized dopant species ratio of ∼8.5:1 for all film thicknesses studied. For solution doping, the dopant solution concentration must be adjusted depending on the polymer film thickness.

We also find that both solution and evaporation sequential doping can effectively dope very thick semiconducting polymer films. When we started this study we expected that evaporation doping would be ineffective for thicker films because the vertical distribution of the dopant would be limited by molecular diffusion, yielding high dopant concentrations near the top surface and a deficit of doping near the substrate. Surprisingly, however, our UV−vis, conductivity, and QCM measurments all indicate that for a wide range of polymer film thicknesses the extent of uniform chemical doping by evaporation only levels off after a monomer unit:dopant ratio of ∼8.5:1 is reached. Both the evaporation and the solution methods can create 400 nm thick doped P3HT films with electrical conductivities of ∼5 S/cm and thermoelectric power factors near 2 μW/mK^2; these same properties can be maintained for films as thick as 2 μm when doped via the solution method.

In addition, we find using grazing-incidence wide-angle X-ray scattering (GIWAXS) that doping by either method increases P3HT crystalline coherence lengths, particularly for the evaporation-doped films: crystallinity of the doped film is important with dopants such as F_4TCNQ in order to keep the dopant anion as far as possible from the polaron on the polymer backbone.[24,55] When the doping process is optimized by either the solution or evaporation sequential methods we see that the amplitude ratio of the P3HT neutral to F_4TCNQ anion/P2 polaron optical absorption peaks is near 1:1, providing a simple guideline to achieve optimal doping when the evaporation thickness cannot be easily controlled. Overall, we conclude that both solution- and evaporation-based doping methods are well suited to achieve high doping concentrations for applications across a wide range of polymer film thicknesses.

2. EXPERIMENTAL METHODS

All materials and solvents were purchased commercially and used as received. Electronic-grade P3HT was purchased from Rieke Metals, and F_4TCNQ was purchased from TCI America. Please see the Supporting Information (SI) for more details.

P3HT solutions at concentrations of 0.5%, 2%, and 5% weight/volume (w/v) were prepared by dissolving 5, 20, and 50 mg P3HT in 1 mL of *o*-dichlorobenzene, respectively. The solutions were heated and stirred at 65 °C to fully dissolve the polymer, and the solutions were cooled to room temperature before use. Films were prepared in a N_2 atmosphere by spin casting the P3HT solutions onto glass substrates at 1000 rpm for 60 s followed by 3000 rpm for 5 s. With this spin-casting condition, the 0.5%, 2%, and 5% w/v P3HT solutions yielded 25, 110, and 400 nm thick films, respectively. Films that were 2 μm thick were prepared by drop casting 30 μL of a 2% w/v P3HT solution onto glass substrates, which were then slow dried by being placed onto a small, covered Petri dish for 2 days. Thickness measurements were carried out using a Dektak 150 profilometer. UV−vis absorption spectra were collected using a Lambda 25 UV−visibile spectrophotometer, and Fourier transform infrared (FTIR) spectroscopy data were acquired for films prepared on KBr plates using a Jasco FT/IR-420 spectrophotometer.

We performed our evaporation sequential doping via controlled thermal evaporation. F_4TCNQ was thermally evaporated onto pre-cast P3HT films using an Angstrom Engineering Nexdep thermal evaporator, in which the F_4TCNQ powder was placed into an alumina crucible that was resistively heated at pressures below 1×10^{-6} Torr to induce sublimation. The pre-cast P3HT films were fixed to a rotating sample stage that was actively cooled using ∼15 °C chilled water. The evaporation rate was held constant at 0.5 Å/s, and the thickness of evaporated dopant was monitored using a quartz crystal microbalance located next to the sample holder. For all of the data presented here, the doped polymer films were characterized immediately (≤1 h) after treating with dopant from either the vapor or the solution phase; however, no changes in conductivity, spectroscopy, or other factors were observed as a function of time after doping if the films were kept under inert atmosphere at room temperature, indicating that subsequent diffusion of the dopant did not take place.

Determination of the P3HT monomer to dopant ratio required measuring the mass density of both pristine P3HT films and pure evaporated films of F_4TCNQ, which was carried out using a previously reported method.[56] The mass density of evaporated F_4TCNQ also was verified using a fresh quartz crystal microbalance (QCM) and surface profilometer. We found that the mass density of evaporated F_4TCNQ is only 0.77 ± 0.06 g/cm^3, about one-half that of the single-crystal density; a more detailed discussion of how we determined the precise amount of F_4TCNQ deposited by evaporation can be found in the SI. Solution sequential doping proceeded via spin coating solutions of F_4TCNQ dissolved in dichloromethane (DCM) at specified concentrations onto pre-cast P3HT films at 4000 rpm for 10 s.

Grazing incidence wide-angle X-ray scattering (GIWAXS) experiments were performed at the Stanford Synchrotron Radiation Lightsource on beamline 11-3 using an X-ray wavelength of 0.9742 Å, an incident angle of 0.12°, and a sample to 2-D charge-coupled device distance of 250 mm. All samples were irradiated for 90 s. Two-dimensional diffractograms were radially integrated from 0° to 180° for full integration, 0−10° for in-plane curves, and 80−90° for out-of-plane curves. Curves were thickness normalized based on the pre-doping film thickness. This normalization was chosen

DOI: 10.1021/acs.jpcc.9b05069
J. Phys. Chem. C 2019, 123, 22711−22724

because only the polymer thickness contributes to the diffraction intensity.

Four-point-probe-based electrical conductivity measurements were performed under ambient conditions on samples fabricated as described above using the Van der Pauw geometry,[57] with silver paste electrodes placed at the corners of the 1.5 × 1.5 cm square samples as in our previous work.[23,24] Electrical conductivities were determined by measuring the film thickness and sheet resistance, and the electrical conductivity was determined by dividing the reciprocal of the measured sheet resistance by the measured thickness of the doped film in centimeters.

For measurements of the thermovoltage/Seebeck coefficient, the samples were prepared in the same way as for the electrical conductivity measurements except the electrodes were fabricated by evaporating 15 nm of molybdenum oxide (MoO_3) to reduce the contact resistance followed by 60 nm of silver; these electrodes had a 6.6 mm spacing. The samples were placed at the interface of two commercial thermoelectric devices to establish a temperature difference between the two electrodes, generating a thermovoltage. We measured the thermovoltage generated at applied temperature differences ranging from 2 to 9 °C and calculated the Seebeck coefficient as the slope of the best-fit line of the thermovoltage vs temperature difference. Details of our home-built thermoelectric characterization setup and data analysis are further described in the SI.

3. RESULTS AND DISCUSSION

The main goal of this work is to understand the evaporation and solution sequential doping methods by comparing them on the same pre-cast conjugated polymer films using the same dopant. We seek to better understand any trade-offs that may exist between the two doping methods and describe under what conditions, if any, one method may be favored over the other. For both types of sequential doping we investigate the limit of thick films, which are expected to function better for many applications, including thermoelectrics. The evaporation doping literature has only explored film thicknesses of a few tens of nanometers, and it is not yet clear if thick polymer films can be fully saturated with dopant by this method. Solution doping has been explored for thicker films using a multilayer method,[45] and more recently, very thick P3HT films (10−40 μm) were demonstrated to be homogeneously doped by soaking in solutions of dopant dissolved in acetonitrile for 72 h.[58] It is still unclear if the method of soaking in a completely orthogonal solvent is reproducible and how this method would extend to solution spin coating, which relies on semiorthogonal swelling solvents in a single, concerted processing step. Here, we show that when properly tuned both the evaporation and the solution sequential doping methods are capable of doping films of surprisingly large thicknesses, yielding comparable conductivities and thermoelectric performance.

3.1. Sequential Doping of P3HT by Thermal Evaporation. We begin our comparison by studying doping via thermal evaporation. For this method, we tracked the extent of doping via the thickness of F_4TCNQ deposited, as measured by a calibrated QCM. For the 25 nm thick polymer films, we explored a range of evaporated dopant thicknesses between 5 and 50 nm. For 110 nm thick P3HT films, we examined dopant thicknesses from 25 to 50 nm. Finally, for 400 nm thick polymer films, our dopant deposition ranged from 25 to 200 nm. The evaporated doping thickness ranges were chosen to span a similar ratio of evaporated dopant thickness to pre-existing polymer film thickness.

The electrical conductivities of our evaporation-doped P3HT films are explored in Figure 2 and Table 1. The blue

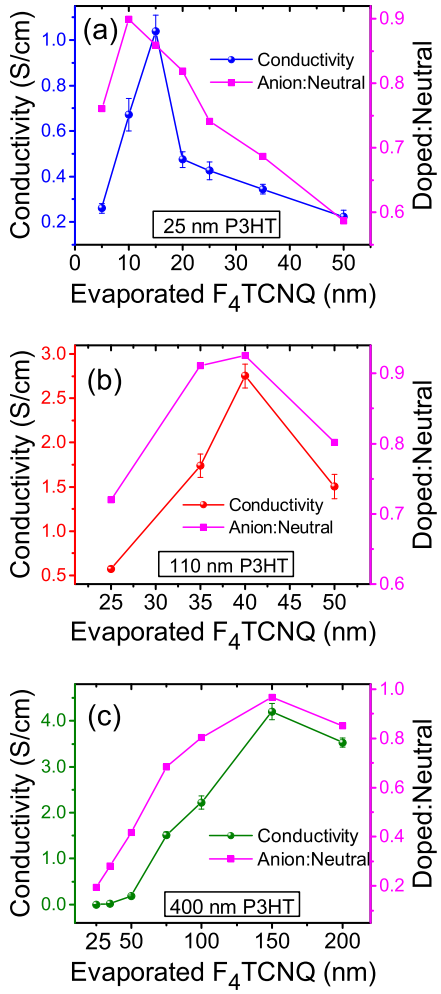

Figure 2. Conductivity (circles) measurements for (a) 25 nm pre-cast P3HT films (blue), (b) 110 nm pre-cast P3HT films (red), and (c) 400 nm pre-cast P3HT films (green) doped with different evaporated thicknesses of F_4TCNQ. Ratio of the optical absorbance at 1.6 eV to that at 2.4 eV (corresponding roughly to the amount of neutral material) for each film is plotted as the magenta squares (right axis); cf. Figure 3. The optical absorption ratio empirically tracks the conductivity and reaches a peak of ∼0.9 at the optimal conductivity.

circles/lines in Figure 2a show that the conductivity of 25 nm pre-cast P3HT films is low when only small amounts of evaporated F_4TCNQ are employed, reaches a maximum with 15 nm of evaporated F_4TCNQ, and then decreases upon evaporation of additional dopant. For 110 nm thick P3HT films, the red circles/lines in Figure 2b show that the optimal conductivity is reached using 40 nm of evaporated dopant. The increased thickness of dopant required to achieve the optimal conductivity makes sense given the greater pre-cast polymer film thickness: additional dopant is clearly required to optimally dope the additional polymer in the thicker film. For 400 nm thick pre-cast P3HT films, the green circles/lines in Figure 2c show that 150 nm of evaporated F_4TCNQ is needed to achieve the optimal conductivity. To our knowledge, this represents the first time a P3HT film of this thickness has

DOI: 10.1021/acs.jpcc.9b05069
J. Phys. Chem. C 2019, 123, 22711−22724

Table 1. Summary of the Conductivity for Sequential Doping of Pre-cast P3HT Films with Different Thicknesses[a]

pre-cast P3HT (nm)	evaporated F_4TCNQ (nm)	doped P3HT film thickness (nm)	conductivity (S/cm)	monomer:dopant ratio[b]
25	5	25 ± 5	0.26 ± 0.02	N/A
	10	26 ± 5	0.67 ± 0.07	17 ± 1
	15	27 ± 5	1.04 ± 0.07	8 ± 1
	20	33 ± 5	0.47 ± 0.03	5 ± 1
	25	45 ± 5	0.43 ± 0.04	4 ± 1
	35	53 ± 5	0.34 ± 0.02	2 ± 1
	50	70 ± 5	0.22 ± 0.03	2 ± 1
110	25	142 ± 5	0.57 ± 0.03	16 ± 1
	35	145 ± 5	1.74 ± 0.13	11 ± 1
	40	149 ± 5	2.75 ± 0.14	9 ± 1
	50	154 ± 5	1.50 ± 0.14	7 ± 1
400	25	403 ± 5	0.00041 ± 0.00004	58 ± 4
	35	407 ± 5	0.019 ± 0.003	38 ± 3
	50	430 ± 5	0.18 ± 0.02	25 ± 3
	75	441 ± 5	1.52 ± 0.06	16 ± 1
	100	480 ± 5	2.22 ± 0.14	12 ± 1
	150	512 ± 5	4.20 ± 0.17	8 ± 1
	200	564 ± 5	3.52 ± 0.10	6 ± 1

[a]The conductivity values were calculated using the measured sheet resistance and thickness of the doped films. [b]These values were calculated after subtracting initial 6 nm of overhead.

been successfully doped to saturation levels by the evaporation method. Previous work has shown that evaporated bulky dopants that are larger than F_4TCNQ can effectively diffuse through P3HT at room temperature but only for 50 nm thick P3HT films.[59] Our results here show that this diffusion holds for films at least eight times as thick.

Although we could have explored thicker films via evaporation sequential doping, we did not examine this limit since reaching the optimal conductivity would likely require evaporating hundreds of nanometers of F_4TCNQ, which becomes cost prohibitive. Additionally, previous work indicates that evaporated F_4TCNQ better penetrates P3HT films if the temperature of the film is raised during evaporation, although it is important to note that excessive heat can de-dope polymer films.[60,61] The data in Figure 2 were taken on films that were actively cooled and held at 15 °C during evaporation. This suggests that evaporation doping should be readily applicable to even thicker films if heating was applied to increase the solid-state diffusion of the dopant into the polymer.

The conductivity values shown in Figure 2 were calculated from the measured electrical sheet resistance using the measured film thickness after doping. In the limit of evaporating a large amount of dopant, enough material was added that the thickness of the film increased significantly after doping. For example, Table 1 shows that the pre-cast 400 nm thick P3HT with the optimal 150 nm of evaporated F_4TCNQ becomes 512 nm thick after doping. We surmise that at the highest evaporated doping thicknesses not all of the dopant participates in the electrical conduction of the films; thus, in some sense, the "conductive thickness" of the doped film is at most only that of the original pre-cast P3HT polymer. This strongly suggests that at the point of maximum conductivity the largest possible number of P3HT units are doped and that addition of more dopant accomplishes little other than increasing the film thickness. As a result, the conductivity begins to decrease past the optimal evaporated dopant thickness simply because of the change in thickness.

Figure 2 and Table 1 also show that we obtain higher maximum conductivities with increasing thickness of the pre-cast P3HT films. As we will discuss further below, this is because the doped thicker films have a larger crystalline coherence length: this produces more delocalized carriers with higher mobilities by helping to increase the distance between the dopant counterion and the conductive hole on the polymer backbone.[24,55]

To gain further insight into the changes taking place in our P3HT films upon evaporation doping, Figure 3 shows the UV−vis absorption spectrum of each of the films whose conductivities were explored in Figure 2. The spectroscopy of F_4TCNQ-doped P3HT films has been explored previously by many groups,[18,23,24,41,44,62] and we show a reference spectrum of a doped film assigning the various features in the SI. For purposes of the discussion here, we will focus on the P3HT neutral exciton absorption peak spanning the region from 2.0 to 2.8 eV and the overlapping P3HT P2 polaron and F_4TCNQ anion absorption peaks near 1.6 eV.[23,62]

Figure 3 shows that for all three pre-cast P3HT film thicknesses, as the amount of evaporated dopant is increased, the amplitude of the P3HT neutral exciton absorption decreases while the amplitude of the overlapping P2 polaron and dopant anion absorption bands concomitantly increases. Moreover, the data also show that once we have passed the point of optimal conductivity for each film, a broad absorption centered near ∼3.1 eV appears due to the presence of neutral F_4TCNQ; the SI shows the absorption spectrum of a pure film of evaporated F_4TCNQ for comparison. Figure 3 thus indicates that once the optimal conductivity is achieved, additional F_4TCNQ does little except cake onto the surface of the film.

Figure 3 also shows that for all three pre-cast P3HT film thicknesses the absorption spectra of the doped films with the optimal amount of evaporated F_4TCNQ for the best conductivity are essentially identical (other than their absolute absorptivities). In particular, we empirically see that the optimally doped films always have a roughly 0.9:1 ratio of the absorbance at 1.6−2.4 eV: these two energies, respectively, correspond roughly to the amounts of doped and neutral material in the film. We note that deconvoluting the

DOI: 10.1021/acs.jpcc.9b05069
J. Phys. Chem. C 2019, 123, 22711−22724

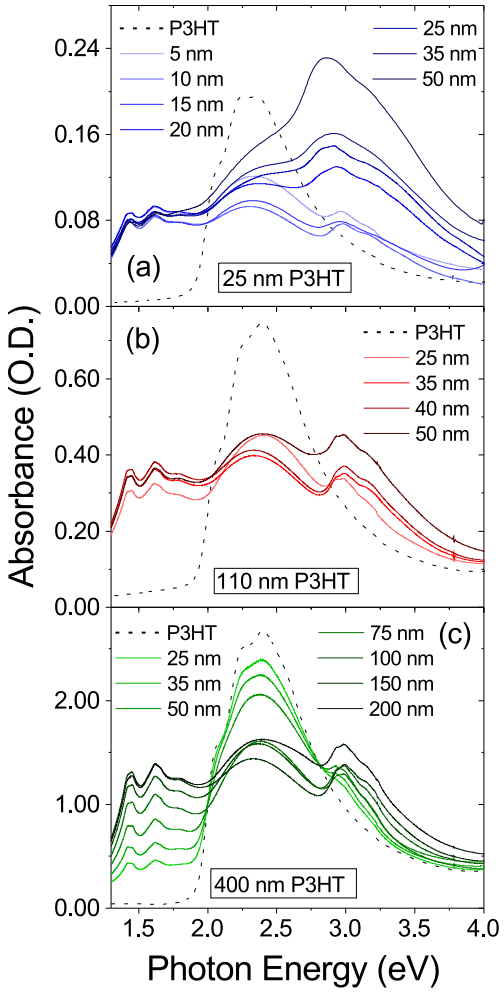

Figure 3. UV−vis absorbance spectra for (a) 25 nm pre-cast P3HT films (blue), (b) 110 nm pre-cast P3HT films (red), and (c) 400 nm pre-cast P3HT films (green) doped with varying thicknesses of evaporated F_4TCNQ; more saturated/darker colors correspond to thicker amounts of evaporated dopant. As the pre-cast P3HT film thickness is increased, an increasing thickness of evaporated F_4TCNQ is required to effectively dope the film. At the F_4TCNQ thickness for optimal electrical conductivity, the ratio of the absorbance at these two energies (plotted in Figure 2) is ∼0.9:1. For all three P3HT film thicknesses, once the optimal conductivity point is passed a new absorbance feature at 3.1 eV due to the presence of neutral F_4TCNQ grows in, indicating that the ability to dope the film is saturated.

overlapping absorbances in this region[43] can be challenging because the spectrum and absorptivity of the polaron and anion species are environment dependent,[23] but we see that the absorption ratio at these two wavelengths serves as an excellent proxy for determining the optimal degree of doping. We plot the ratio of the absorbance at 1.6 and 2.4 eV for each of our evaporated doped films as the magenta squares/lines in Figure 2. Below, we will show that optimally doped films created by solution sequential doping also have a similar absorbance ratio at these two energies. This indicates that this ratio corresponds to optimal doping in all situations for this materials combination. This suggests that when the amount of evaporated dopant cannot be readily controlled (such as in a homemade sublimation setup), one could use the empirically determined absorbance ratio at these two wavelengths as a useful proxy for determining the optimal amount of F_4TCNQ needed to dope a given P3HT film.

As summarized in Table 1, the 25, 110, and 400 nm pre-cast P3HT films require 15, 40, and 150 nm of evaporated F_4TCNQ, respectively, in order to achieve their optimal conductivity. When we examine the ratio of optimal evaporated dopant thickness to pre-cast polymer film thickness we see that it is 0.36 and 0.38 for the 110 and 400 nm pre-cast films, respectively. This strongly suggests that there is an optimal doping ratio that is independent of the polymer film thickness. The 25 nm thick pre-cast film, however, has a much higher evaporated dopant:polymer thickness ratio (∼0.6) at the optimal conductivity point.

This discrepancy in dopant/polymer thickness ratio for the 25 nm P3HT film likely results from structural transitions that occur when P3HT is doped with F_4TCNQ.[18] As dopant is introduced into the polymer, it is well documented that the P3HT lamellar spacing becomes larger and the $\pi-\pi$ stacking distance decreases,[23,24] a change that can be attributed to a reorientation of the P3HT chains with respect to the unit cell to accommodate the presence of the dopant in the lamellar region of the film.[18] This makes it possible that there exists a threshold or "overhead" thickness of evaporated dopant that is required to induce or nucleate this structural transition, as discussed further in the SI. It is also possible that this overhead thickness is required for filling trap states in the polymer film before an appreciable number of free carriers can be formed, although this would suggest that the overhead thickness would depend on the film thickness. An explanation in better agreement with our observations is that structural reorganization proceeds in a way similar to seeded crystal growth, where a minimum crystal size is required to initiate the process, at which point the structural reorganization may self-propagate as new dopants are added. We find that if the required "overhead" thickness of evaporated F_4TCNQ is 6 nm we obtain an identical dopant-to-polymer thickness ratio of ∼1/3 for all three P3HT film thicknesses, as shown in the SI.

We can take this idea of an optimal thickness ratio a step further and analyze the ratio of thiophene monomer units to ionized dopant molecules at the optimal doping concentration. Typically, this ratio has only been determined at very low doping levels when the dopant and polymer species were codissolved at carefully prescribed concentrations. At higher dopant concentrations, this ratio has been estimated based on the optical absorption of the polaron in the infrared region of the spectrum (the so-called P1 absorption).[44,63] Unfortunately, as mentioned above, the spectral position, shape and intensity of the P1 polaron absorption band changes with the degree of P3HT crystallinity because of a change in the average distance between the polaron and the counterion,[24,55] and the P2 polaron absorption overlaps with that of the F_4TCNQ anion. This makes the reliable determination of stoichiometric dopant ratios by optical methods a challenging task. This is especially true near the limit of saturation doping levels when both trapped and free polarons can be present.[23,64]

However, because our vapor-doping process uses a QCM thickness monitor in situ, we have explicit knowledge of the mass of the added dopant during thin-film deposition. As described in the SI, by measuring the evaporated F_4TCNQ and spin-coated P3HT film mass densities we are able to determine the dopant/polymer stoichiometry based on the evaporated dopant thickness. The stoichiometric ratios for each evaporation are summarized in Table 1. We find that when excluding

DOI: 10.1021/acs.jpcc.9b05069
J. Phys. Chem. C 2019, 123, 22711−22724

the measured "overhead" thickness of 6 nm, the optimum ratio of P3HT thiophene units to ionized F_4TCNQ dopants is ~8.5:1 for all P3HT film thicknesses.

On the basis of this information, we can draw two important conclusions about the evaporation doping process. First, it appears that small molecule dopants like F_4TCNQ are capable of interpenetrating films of P3HT of essentially any thickness. Second, it appears that there is little point to further doping beyond the optimal ratio of ~8.5:1 thiophene units per ionized F_4TCNQ molecule. For dopant densities higher than optimal, we see an increase in absorption of the neutral F_4TCNQ species located at ~3.1 eV, suggesting once saturation doping levels are reached much of the additional F_4TCNQ does not undergo charge transfer. This observation is consistent with previous work that suggests at higher doping levels there is an increase in the creation of trapped carriers, suggesting that the optimal ratio is where the polymer crystallites become full with dopant.[64]

3.2. Sequential-Doping of P3HT by Solution Processing. We continue our comparison of sequential doping methods in this section by exploring the properties of P3HT films doped via solution sequential doping. This involves spin-coating solutions of F_4TCNQ dissolved in dichloromethane at different concentrations on top of pre-cast P3HT films of different thicknesses. DCM is known to swell P3HT films without dissolving them, and it also has a reasonable solubility for F_4TCNQ, allowing mass action to drive the dopant into the swollen polymer underlayer.[26] In previous work we have successfully used this method to dope P3HT films of roughly 100 nm thickness with F_4TCNQ,[23−26] and another group developed a layer-by-layer version of solution doping to produce thicker doped films for thermoelectrics.[45]

We begin by investigating how the use of different F_4TCNQ solution concentrations (0.01, 0.1, and 1 mg/mL) influence the resultant electrical conductivity of doped P3HT films with different thicknesses. Figure 4 shows that when using a 0.01 mg/mL F_4TCNQ solution (orange diamond) we are able to measure the conductivity of a pre-cast 25 nm thick P3HT film, but thicker films show no measurable conductivity as they are highly under-doped. When we increase the dopant concentration to 0.1 mg/mL (maroon squares), we see respectable conductivities (≤1 S/cm) for pre-cast 25, 110, and 400 nm thick P3HT films. Not until we use a 1 mg/mL F_4TCNQ solution, which is close to the F_4TCNQ solubility limit in DCM, we can effectively dope P3HT films with thicknesses ranging from 25 nm to 2 μm; these films all have conductivities above 1 S/cm.

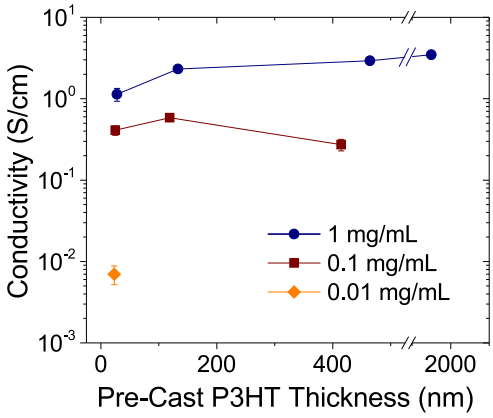

Figure 4. Conductivity measurements for solution-doped pre-cast P3HT films ranging in thickness from 25 to 2000 nm. Films are solution doped with 0.01 (orange diamond), 0.1 (maroon squares), or 1 mg/mL (navy circles) solutions of F_4TCNQ in DCM. Film conductivity increases with increasing F_4TCNQ concentration until an optimal value is reached. Note the *x*-axis scale break between 525 and 1900 nm.

These results demonstrate that solution sequential doping can be used in a single step to optimize the conductivity of even very thick conjugated polymer films. Similar to our evaporation results, the thickest pre-cast P3HT films have the highest electrical conductivities, which we attribute below to greater polymer ordering and thus hole mobility. Although ~1 μm thick films of P3HT have previously been doped with tetrabutylammonium salts,[65] our results here represent, to the best of our knowledge, the thickest reported films of P3HT doped with F_4TCNQ.

Figure 5 presents the UV−vis absorption spectra of the solution-doped films, which show noticeably similar trends compared to the evaporation-doped films (Figure 3): as the dopant concentration increases, the neutral P3HT peak intensity decreases while that of the F_4TCNQ anion/P2 polaron peak increases. Figure 5a shows that 25 nm thick pre-cast P3HT films are already highly doped even when using a low solution F_4TCNQ concentration of 0.01 mg/mL. When the dopant solution concentration is increased to 1 mg/mL, we observe significant absorbance at 3.1 eV from neutral F_4TCNQ, indicating we are past the optimal doping point and have oversaturated the films with F_4TCNQ. For 110 nm thick pre-cast P3HT films, Figure 5b shows a similar trend, but at low dopant concentrations, the extent of doping is reduced. This fits with our expectation that additional polymer material requires additional dopant to achieve the same doping levels. Figure 5c indicates that for 400 nm thick pre-cast P3HT films the extra polymer material requires the use of the higher concentration 1 mg/mL dopant solution to achieve sufficient doping levels. We were unable to perform UV−vis spectroscopy on 2 μm thick P3HT films because their optical density exceeds 10.

Although the concentration range investigated here is more coarse grained than that explored for vapor doping, it is worth discussing some final similarities and differences between the two methods. First, in the case where dopant is in high excess relative to the polymer we see very similar absorption features in the UV−vis spectra. This is most clearly illustrated in Figures 3a and 5a, where excess dopant produces very similar absorption profiles, independent of doping method. One marked difference we might expect between the two methods concerns the need for the overhead thickness to induce structural reordering, as in the case of vapor doping. Because polymer films swell during the solution doping process it is plausible that the swelling solvent provides the impetus for the needed structural reordering, negating the need for an overhead amount of dopant material. Again, adequately exploring the analogous doping regime for solution processing would require investigating a more finely spaced concentration range, and we leave this open to future work.

When we examine the UV−vis spectra in more detail we see that the ratio of the doped material absorption peak at 1.6 eV to the neutral P3HT absorption peak at 2.4 eV is ~1.1:1, which is very similar to the optimal ratio of ~0.9:1 that we saw with evaporation doping. We note that the absorbance peak ratio for the 25 nm thick film is lower, but this likely results

DOI: 10.1021/acs.jpcc.9b05069
J. Phys. Chem. C 2019, 123, 22711−22724

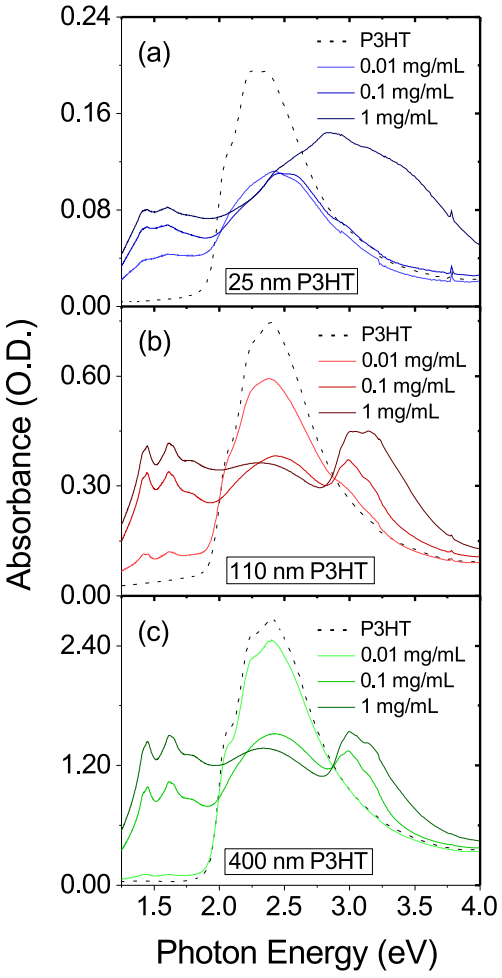

Figure 5. UV−vis absorption spectra for (a) 25 nm pre-cast P3HT films (blue), (b) 110 nm pre-cast P3HT films (red), and (c) 400 nm pre-cast P3HT films (green); as with Figure 3, more saturated/darker colors correspond to increased dopant concentrations of 0.01, 0.1, and 1 mg/mL. As the thickness of P3HT increases, an increasing concentration of F_4TCNQ is required to effectively dope the film, as indicated by the decrease of the P3HT neutral peak near 2.4 eV and the increase of the F_4TCNQ anion/polaron P2 peak near 1.6 eV. As with the evaporated doped films, the optimal electrical conductivity occurs when the doped:neutral ratio is ∼1.1. For all films in this thickness range, the doping becomes saturated at higher concentrations, as evidenced by the appearance of absorbance due to neutral F_4TCNQ peak near 3.1 eV.

from overlap of the neutral P3HT peak with the tail of the neutral F_4TCNQ absorption. Thus, the UV−vis absorption spectrum can serve as a guide to finding the optimal doping concentration for electrical conductivity by roughly matching the intensities of the neutral and doped P3HT absorbance peaks. This result follows in the same manner as our UV−vis results for evaporation-doped films, where the same ratio was observed for optimal electrical conductivity.

3.3. Structural and Infrared Characterization of Vapor- and Solution-Doped P3HT Films. In order to better understand the relationship between film structure and the conductivity of our doped and undoped P3HT films, we used 2-D grazing-incidence wide-angle X-ray scattering (GIWAXS) to study films doped by both evaporation and solution sequential doping. In the data shown below we study P3HT films at their optimal doping level for conductivity, as determined by the data in Figures 2 and 4.

Undoped P3HT is well known to prefer an edge-on orientation in films: the π-stacking or (010) diffraction peak appears in the in-plane direction, and the lamellar or side-chain spacing (100) peak appears in the out-of-plane direction. Figure 6 shows representative 2-D diffractograms for 110 nm

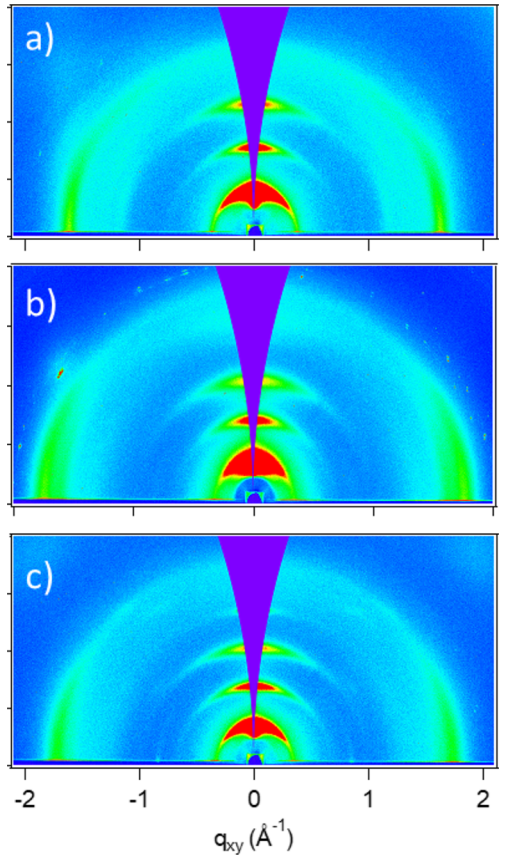

Figure 6. Representative 2-D diffractograms of 110 nm thick P3HT films that are (a) undoped, (b) doped with F_4TCNQ via solution sequential processing, and (c) doped with F_4TCNQ via thermal evaporation. These results demonstrate that the natural edge-on orientation of the P3HT chains in undoped films is maintained following both methods of sequential doping.

thick P3HT films. The data demonstrate that, as expected, the pre-cast films (Figure 6a), solution-doped films (Figure 6b), and evaporation-doped films (Figure 6c) have a preferentially edge-on orientation. We also show in Figures S5, S7, and S8 of the SI that edge-on orientation is maintained for all other P3HT thicknesses of pre-cast and sequentially doped films.

Previous work has shown that increased P3HT relative crystallinity (as measured by the (100) peak intensity) is correlated with increased conductivity in F_4TCNQ-doped films.[23−25,41,43] The origin of this increase lies in the fact that F_4TCNQ molecules located within crystalline domains sit between the side chains in the lamellar region and are thus held fairly far from the polaron on the P3HT backbone. This distance decreases coulomb attractions between the polaron and the counterion, which is particularly important given the low dielectric constant of most conjugated polymers, thereby resulting in more mobile charge carriers.[55]

DOI: 10.1021/acs.jpcc.9b05069
J. Phys. Chem. C 2019, 123, 22711−22724

Table 2. Summary of the Thickness-Normalized GIWAXS Data for Pure P3HT, Solution-Doped P3HT, and Vapor-Doped P3HT Films

pre-cast P3HT (nm)	doping method	(100) peak position ($Å^{-1}$)	relative (100) peak area	(200) peak position ($Å^{-1}$)	relative (200) peak area	coherence length (nm)	(100):(200) peak area ratio
25	none	0.39	1.0	0.78	1.0	9.3	29:1
	solution	0.37	1.2	0.72	2.0	8.8	17:1
	vapor	0.35	0.92	0.70	2.1	9.2	12:1
110	none	0.40	0.73	0.78	1.1	13	20:1
	solution	0.36	0.97	0.70	3.0	9.0	10:1
	vapor	0.35	0.55	0.69	1.8	14	8:1
400	none	0.40	0.83	0.78	1.3	11	18:1
	solution	0.35	0.55	0.69	1.9	9.2	8:1
	vapor	0.35	0.36	0.69	1.4	14	7:1
2000	none	0.40	0.51	0.80	0.83	13	17:1
	solution	0.35	0.34	0.69	1.3	12	8:1

We note that simply integrating the (100) scattering peak is not the ideal way to determine the relative crystalline fraction of a P3HT film because other effects (overall structure factor, etc.) can modify this value, particularly for films with very different thicknesses. Table 2 summarizes the GIWAXS data for all of our pristine and sequentially doped P3HT films. These data show that based simply on the thickness-normalized integrated (100) peak areas, the thicker and more conductive doped films in fact have lower relative crystallinity. Moreover, the vapor-doped films show lower integrated (100) peak areas than the thickness-matched solution-doped films, despite the fact that vapor doping produces more conductive films (Figures 2 and 4).

Since diffraction peak area alone cannot explain the conductivity trends we observe with the doping method or film thickness, we also investigated the relative degree of order of the crystalline regions, which is reflected in the GIWAXS crystalline coherence length and relative overtone strength.[66−68] Figure 7 shows that doping by either sequential method causes the lamellar (h00) peaks to shift to lower q, which corresponds to a larger d spacing that better accommodates the F_4TCNQ anion, as expected.[18] However, the insets of Figure 7a and 7b demonstrate that vapor doping of P3HT also causes a (400) lamellar overtone to appear, which is particularly evident in thicker films. There is no sign of a new (400) peak for the equivalent solution-doped P3HT samples, in agreement with previously published work,[23−25,33,41,42] indicating that this additional order is induced only by the vapor doping process.

Using the widths of the (h00) overtones we calculated crystallite size or crystallite coherence lengths from the Scherrer equation.[69,70] The results in Table 2 show that for films thicker than 25 nm, vapor doping results in an increase in domain sizes compared to both solution-doped P3HT films and the original undoped P3HT films. For example, the vapor-doped samples where the (400) peak is observed have a crystalline coherence length calculated from the diffraction peak width of 14 nm, while our solution-doped films of equivalent thickness demonstrate a coherence length of only 9 nm. This increased coherence length further corroborates the conclusion that the vapor-doped samples are more ordered than the solution-doped samples. The decrease in peak width and the increase in the number of observable overtones together indicate that doping increases the long-range order of P3HT films and that evaporative doping increases the long-range order of P3HT to a greater extent than solution doping.

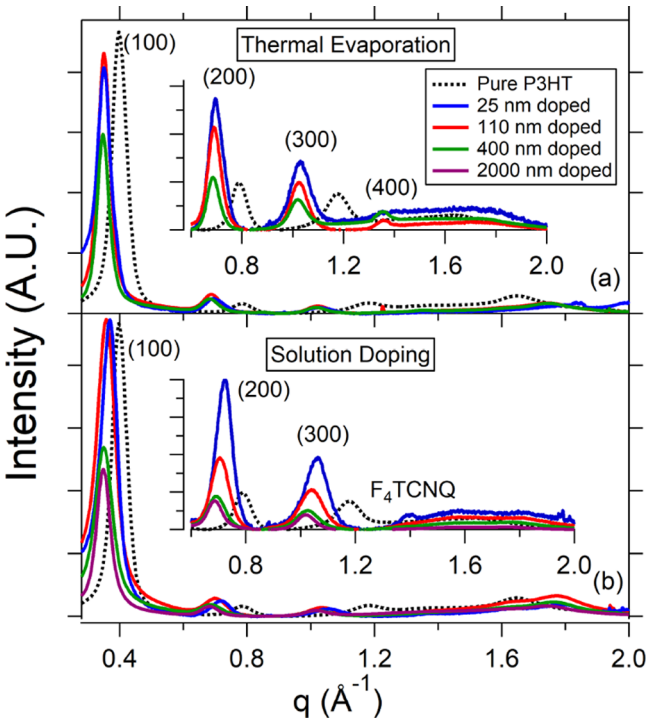

Figure 7. Full integrations of thickness-normalized 2-D GIWAXS diffractograms of P3HT films doped with F_4TCNQ via (a) thermal evaporation and (b) solution sequential processing. Data for undoped P3HT (dashed black curve) is shown for reference. Out-of-plane integrations are included in the expanded insets for clarity. Data show that 25 (blue) and 110 nm (red) films both largely maintain their original crystallinity after doping. For the 110 and 400 nm (green) vapor-doped films, a (400) overtone appears, indicating improved long-range order that correlates with higher carrier mobility and thus conductivity.

Figure 7 and Table 2 also show that although the peak widths are somewhat broader for solution-doped films compared to both undoped and vapor-doped films, the relative intensities of the overtone peaks is even higher than those from the vapor-doped material. This suggests that for the P3HT/F_4TCNQ system it is not the overall crystalline fraction that contributes to increased conductivity but rather increased long-range ordering within the crystalline regions that correlates with increased conductivity, presumably because this best increases the average polaron-to-counterion distance.[55]

DOI: 10.1021/acs.jpcc.9b05069
J. Phys. Chem. C 2019, 123, 22711−22724

To better explore the correlation between film structure and the resultant carrier properties we measured the IR absorption spectrum of the P1 polaron transition for our 110 and 400 nm pre-cast P3HT films. We chose conditions for both solution and evaporation doping to achieve the optimal electrical conductivity at each thickness. Figure 8 shows that for the 400

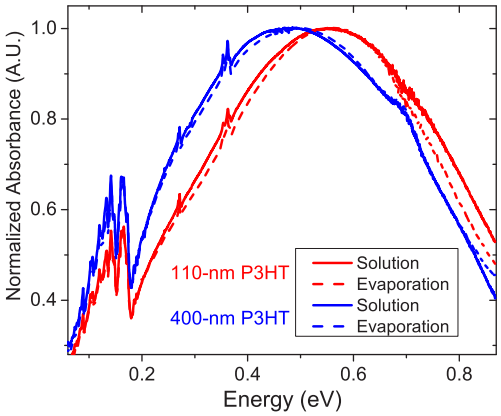

Figure 8. Absorption spectra of the P1 polaron transition for the doped 110 (red) and 400 nm (blue) pre-cast P3HT films. Films are doped by solution (solid lines) and evaporation (dashed lines) sequential doping; doping conditions were selected to optimize the electrical conductivity. P1 band for both the solution and the evaporation sequentially doped 400 nm pre-cast P3HT films is red shifted, indicating greater polymer ordering that is correlated with a higher hole mobility.

nm thick pre-cast P3HT films (blue curves) the main P1 band is red shifted and the IR-active vibrations (IRAVs, which occur below 0.18 eV) have a higher intensity compared to the 110 nm thick pre-cast films (red curves), independent of processing method.[71] A red-shifted P1 band and higher absorption IRAV band are known to correlate with increased polaron delocalization and hence higher carrier mobility.[24,55,72−74] Thus, we see a direct correlation between the degree of polaron delocalization and conductivity, explaining why thicker films in general have higher conductivities.

3.4. Thermoelectric Properties of P3HT Films Prepared by Evaporation and Solution Sequential Doping. Having compared two methods for effectively sequentially doping P3HT films of varying thickness, we now turn to investigating how F_4TCNQ-doped P3HT films fabricated by the different routes function as thermoelectric materials up to 2 μm thick. Figure 9 presents the thermoelectric properties of the evaporation-doped (black squares) and solution-doped (red circles) P3HT films that yielded the highest electrical conductivities for each pre-cast film thickness. Figure 9a shows that the electrical conductivity increases with increasing pre-cast P3HT film thickness for both doping methods. As mentioned above, this is because the thicker P3HT films have a higher degree of delocalization, yielding higher mobility carriers. The evaporation-doped samples yield slightly higher conductivities at the same film thickness, which is due to slightly increased long-range order in the evaporation-derived materials. The UV−vis absorption spectra of these optimal-conductivity films are all quite similar, as shown in the SI.

Figure 9b shows the Seebeck coefficients of the doped polymer films, which are determined by the magnitude of the thermovoltage produced for a given temperature gradient. The

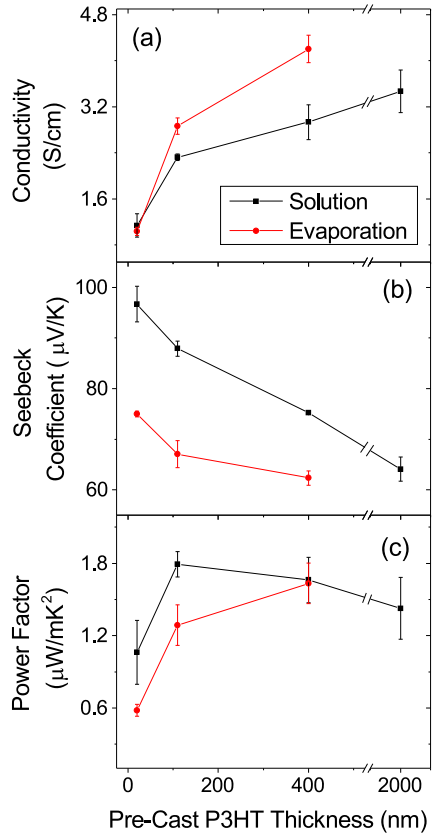

Figure 9. Thermoelectric properties of 25, 110, 400, and 2000 nm pre-cast P3HT films doped with F_4TCNQ by solution (black squares) and evaporation (red circles) sequential processing. Processing conditions for each method were chosen to produce the most conductive films. For evaporation doping, the 25, 110, and 400 nm thick pre-cast P3HT films were doped with 15, 40, and 150 nm of F_4TCNQ, respectively. For solution doping, all P3HT films were doped with a 1 mg/mL F_4TCNQ solution. (a) Thicker P3HT films have higher electrical conductivities than thinner films, and evaporation doping produces slightly higher conductivities than solution doping. (b) Seebeck coefficient of doped P3HT films decreases with increasing film thickness, and solution doping yields slightly higher values than evaporation doping. (c) Thermoelectric power factors of all of our doped P3HT films are similar, indicating that both processing techniques produce films equally well suited for use in thermoelectrics. Note the scale break on the *x*-axis between 525 and 1900 nm.

data show that the Seebeck coefficient decreases for the thicker, more conductive films. This trend agrees with the well-known anticorrelation between electrical conductivity and Seebeck coefficient, where the Seebeck coefficient is seen empirically to vary as electrical conductivity to the 1/4 power,[14,22] as shown in more detail in the SI. Indeed, the Seebeck coefficients for the solution-doped films are higher than those for the evaporation-doped films, as expected from their slightly lower electrical conductivities. Furthermore, we note that the Seebeck coefficients we measure in the tens of μV/K range are consistent with those found in other studies on thinner films of doped polythiophenes.[22,34]

Finally, we calculated the thermoelectric power factor, which is the product of the electrical conductivity and the square of the Seebeck coefficient. The power factor, along with the thermal conductivity and the temperature, is the main measure of thermoelectric efficiency; we show the power factor for our

DOI: 10.1021/acs.jpcc.9b05069
J. Phys. Chem. C 2019, 123, 22711−22724

doped P3HT films in Figure 9c.[14,22] For all film thicknesses that we investigated the devices show similar power factors on the order of 1−2 μW/mK^2. The fact that the power factor holds for the 2 μm thick film shows that solution sequential processing is an effective method for producing organic thermoelectric active layers.

Overall, we see that regardless of doping methodology the thermoelectric properties of solution- and evaporation-doped polymer films are quite similar. Even though the two methods deliver the dopant in different ways, they both preserve the original P3HT film structure by doping in a sequential manner,[23,24,26,33,42] and thus, both offer potential for creating active layers for organic thermoelectrics. Overall, both evaporation and solution doping methods have distinct advantages, and our results show that one can use whichever method best suits the particular device fabrication needs: solution processing benefits from lower cost, while evaporation methods might be more amenable for larger device areas.

4. CONCLUSIONS

In this paper, we demonstrate that sequential processing is a highly effective method for chemically doping conjugated polymer films by performing a direct comparison between identically prepared evaporation- and solution-doped films. Sequential doping starts with a pre-cast polymer film, which is then doped either by thermally evaporating dopant or by spin casting a solution of dopant on top of the polymer film. Both methods have the advantage of leaving the structure of the pre-cast polymer film roughly intact, and thus, the methods give similar electrical conductivities with similar degrees of doping.

One key aspect of this work is our demonstration that both methods can be used to dope very thick semiconductor polymer films. For evaporation sequential doping, we demonstrated the ability to dope films up to 400 nm thick, and the doping of thicker films should be readily possible (particularly if heating is employed to improve diffusion of the dopant into the film), limited only by cost of evaporating large amounts of dopant. For solution sequential doping, we have shown that films up to 2 μm thick can be doped via spin coating in a single processing step.

Evaporation doping results in improved long-range crystallinity, as evidenced by the development of a (400) lamellar overtone in GIWAXS, and increased crystalline coherence lengths, explaining why evaporation doping achieves slightly higher electrical conductivities than solution doping. Evaporation doping requires an "overhead" thickness of ∼6 nm, possibly to induce restructuring of the polymer crystal lattice to accommodate the dopant; once the overhead is complete, the optimal evaporated F_4TCNQ thickness is ∼1/3 the P3HT film thickness, resulting in a thiophene monomer:ionized dopant molecule ratio of ∼8.5:1. Solution doping, on the other hand, allows access to the doping of thicker films with a far more cost efficient use of material. However, finding the optimal solvent to dissolve the dopant and swell, but not dissolve the polymer may not be so straightforward with every polymer:dopant combination.

For both sequential doping methods we find empirically that UV−vis absorption spectroscopy provides a good indication of when the optimal electrical conductivity has been achieved. Here we define optimal as the point where the ratio of the doped to neutral P3HT absorption approaches 1:1. When less dopant than the optimal is used, the films have poor conductivity because much of the polymer remains undoped. When more dopant than optimal is employed, the film conductivity decreases slightly, due to the fact that additional dopant either creates trapped carriers or does not dope at all. The increase in thickness that results from the presence of excess dopant causes a drop in conductivity. Thicker pre-cast P3HT films demonstrate higher electrical conductivities due to greater polymer long-range ordering, which increases the hole mobility.

Upon fabricating thermoelectric devices by both sequential doping methods we find that their thermoelectric properties are quite similar regardless of which method is employed. For each polymer film thickness studied, the power factors fall across only a narrow range. This demonstrates that processing techniques that operate on fundamentally different principles can both be successfully applied to the fabrication of thermoelectric devices. Finally, although we have pushed the limit of sequential doping to 2 μm thick films, it is clear that either technique could potentially be extended to still thicker films, which is an avenue worth exploring in the future.

■ ASSOCIATED CONTENT

Supporting Information

The Supporting Information is available free of charge on the ACS Publications website at DOI: 10.1021/acs.jpcc.9b05069.

Details on the device materials, doping fabrication procedures, UV−vis spectra, grazing incidence wide-angle X-ray scattering (GIWAXS) experiments and analysis, calculation of the F_4TCNQ overhead thickness, determination of the monomer:dopant ratio in evaporation-doped films, conductivity measurements, thermoelectric measurements, and Seebeck empirical power law fitting (PDF)

■ AUTHOR INFORMATION

Corresponding Authors

*E-mail: schwartz@chem.ucla.edu. (B.J.S.)
*E-mail: tolbert@chem.ucla.edu. (S.H.T.)

ORCID

Sarah H. Tolbert: 0000-0001-9969-1582
Benjamin J. Schwartz: 0000-0003-3257-9152

Author Contributions

‡M.T.F. and D.A.S.: These authors contributed equally to this work.

Notes

The authors declare no competing financial interest.

■ ACKNOWLEDGMENTS

This work was supported by the National Science Foundation under grant numbers CBET-1510353 and CHE-1608957.

■ REFERENCES

(1) Kaloni, T. P.; Giesbrecht, P. K.; Schreckenbach, G.; Freund, M. S. Polythiophene: From Fundamental Perspectives to Applications. *Chem. Mater.* **2017**, *29*, 10248−10283.

(2) Krebs, F. C. Fabrication and Processing of Polymer Solar Cells: A Review of Printing and Coating Techniques. *Sol. Energy Mater. Sol. Cells* **2009**, *93*, 394−412.

(3) Li, Y. Molecular Design of Photovoltaic Materials for Polymer Solar Cells: Toward Suitable Electronic Energy Levels and Broad Absorption. *Acc. Chem. Res.* **2012**, *45*, 723−733.

DOI: 10.1021/acs.jpcc.9b05069
J. Phys. Chem. C 2019, 123, 22711−22724

(4) Lu, L.; Zheng, T.; Wu, Q.; Schneider, A. M.; Zhao, D.; Yu, L. Recent Advances in Bulk Heterojunction Polymer Solar Cells. *Chem. Rev.* **2015**, *115*, 12666−12731.
(5) Søndergaard, R.; Hösel, M.; Angmo, D.; Larsen-Olsen, T. T.; Krebs, F. C. Roll-to-Roll Fabrication of Polymer Solar Cells. *Mater. Today* **2012**, *15*, 36−49.
(6) McCulloch, B.; Ho, V.; Hoarfrost, M.; Stanley, C.; Do, C.; Heller, W. T.; Segalman, R. A. Polymer Chain Shape of poly(3-alkylthiophenes) in Solution Using Small-Angle Neutron Scattering. *Macromolecules* **2013**, *46*, 1899−1907.
(7) Spakowitz, A. J.; Wang, Z. G. Exact Results for a Semiflexible Polymer Chain in an Aligning Field. *Macromolecules* **2004**, *37*, 5814−5823.
(8) Deibel, C.; Dyakonov, V. Polymer-Fullerene Bulk Heterojunction Solar Cells. *Rep. Prog. Phys.* **2010**, *73*, 096401.
(9) Duan, C.; Huang, F.; Cao, Y. Recent Development of Push-Pull Conjugated Polymers for Bulk-Heterojunction Photovoltaics: Rational Design and Fine Tailoring of Molecular Structures. *J. Mater. Chem.* **2012**, *22*, 10416.
(10) Giovanella, U.; Botta, C.; Galeotti, F.; Vercelli, B.; Battiato, S.; Pasini, M. Perfluorinated Polymer with Unexpectedly Efficient Deep Blue Electroluminescence for Full-Colour OLED Displays and Light Therapy Applications. *J. Mater. Chem. C* **2013**, *1*, 5322−5329.
(11) Heeger, A. J. 25th Anniversary Article: Bulk Heterojunction Solar Cells: Understanding the Mechanism of Operation. *Adv. Mater.* **2014**, *26*, 10−28.
(12) Céspedes-Guirao, F. J.; García-Santamaría, S.; Fernández-Lázaro, F.; Sastre-Santos, A.; Bolink, H. J. Efficient Electroluminescence from a Perylenediimide Fluorophore Obtained from a Simple Solution Processed OLED. *J. Phys. D: Appl. Phys.* **2009**, *42*, 105106.
(13) Kozma, E.; Mróz, W.; Villafiorita-Monteleone, F.; Galeotti, F.; Andicsová-Eckstein, A.; Catellani, M.; Botta, C. Perylene Diimide Derivatives as Red and Deep Red-Emitters for Fully Solution Processable OLEDs. *RSC Adv.* **2016**, *6*, 61175−61179.
(14) Snyder, G. J.; Toberer, E. S. Complex Thermoelectric Materials. *Nat. Mater.* **2008**, *7*, 105−114.
(15) Sun, J.; Yeh, M. L.; Jung, B. J.; Zhang, B.; Feser, J.; Majumdar, A.; Katz, H. E. Simultaneous Increase in Seebeck Coefficient and Conductivity in a Doped Poly(alkylthiophene) Blend with Defined Density of States. *Macromolecules* **2010**, *43*, 2897−2903.
(16) McGrail, B. T.; Sehirlioglu, A.; Pentzer, E. Polymer Composites for Thermoelectric Applications. *Angew. Chem., Int. Ed.* **2015**, *54*, 1710−1723.
(17) Hwang, S.; Potscavage, W. J.; Nakamichi, R.; Adachi, C. Processing and Doping of Thick Polymer Active Layers for Flexible Organic Thermoelectric Modules. *Org. Electron.* **2016**, *31*, 31−40.
(18) Hamidi-Sakr, A.; Biniek, L.; Bantignies, J. L.; Maurin, D.; Herrmann, L.; Leclerc, N.; Lévêque, P.; Vijayakumar, V.; Zimmermann, N.; Brinkmann, M. A Versatile Method to Fabricate Highly In-Plane Aligned Conducting Polymer Films with Anisotropic Charge Transport and Thermoelectric Properties: The Key Role of Alkyl Side Chain Layers on the Doping Mechanism. *Adv. Funct. Mater.* **2017**, *27*, 1700173.
(19) Kiefer, D.; Yu, L.; Fransson, E.; Gómez, A.; Primetzhofer, D.; Amassian, A.; Campoy-Quiles, M.; Müller, C. A Solution-Doped Polymer Semiconductor:Insulator Blend for Thermoelectrics. *Advanced Science* **2017**, *4*, 1600203.
(20) Yao, H.; Fan, Z.; Cheng, H.; Guan, X.; Wang, C.; Sun, K.; Ouyang, J. Recent Development of Thermoelectric Polymers and Composites. *Macromol. Rapid Commun.* **2018**, *39*, 1700727.
(21) Heremans, J. P. Thermoelectricity: The Ugly Duckling. *Nature* **2014**, *508*, 327−328.
(22) Russ, B.; Glaudell, A.; Urban, J. J.; Chabinyc, M. L.; Segalman, R. A. Organic Thermoelectric Materials for Energy Harvesting and Temperature Control. *Nature Reviews Materials* **2016**, *1*, 1−14.
(23) Scholes, D. T.; Hawks, S. A.; Yee, P. Y.; Wu, H.; Lindemuth, J. R.; Tolbert, S. H.; Schwartz, B. J. Overcoming Film Quality Issues for Conjugated Polymers Doped with F4TCNQ by Solution Sequential Processing: Hall Effect, Structural, and Optical Measurements. *J. Phys. Chem. Lett.* **2015**, *6*, 4786−4793.
(24) Scholes, D. T.; Yee, P. Y.; Lindemuth, J. R.; Kang, H.; Onorato, J.; Ghosh, R.; Luscombe, C. K.; Spano, F. C.; Tolbert, S. H.; Schwartz, B. J. The Effects of Crystallinity on Charge Transport and the Structure of Sequentially Processed F4TCNQ-Doped Conjugated Polymer Films. *Adv. Funct. Mater.* **2017**, *27*, 1702654.
(25) Scholes, D. T.; Yee, P. Y.; Mckeown, G. R.; Li, S.; Kang, H.; Lindemuth, R.; Xia, X.; King, S. C.; Seferos, D. S.; Tolbert, S. H.; et al. Designing Conjugated Polymers for Molecular Doping: The Roles of Crystallinity, Swelling, and Conductivity in Sequentially-Doped Selenophene-Based Copolymers. *Chem. Mater.* **2019**, *31*, 73−82.
(26) Fontana, M. T.; Aubry, T. J.; Scholes, D. T.; Hawks, S. A.; Schwartz, B. J. *Handbook of Organic Optoelectronic Devices*; World Scientific, 2018; Vol. 2; Chapter 8.
(27) Yim, K.-H.; Whiting, G. L.; Murphy, C. E.; Halls, J. J. M.; Burroughes, J. H.; Friend, R. H.; Kim, J.-S. Controlling Electrical Properties of Conjugated Polymers via a Solution-Based p-Type Doping. *Adv. Mater.* **2008**, *20*, 3319−3324.
(28) Zhang, Y.; de Boer, B.; Blom, P. W. M. Controllable Molecular Doping and Charge Transport in Solution-Processed Polymer Semiconducting Layers. *Adv. Funct. Mater.* **2009**, *19*, 1901−1905.
(29) Duong, D. T.; Wang, C.; Antono, E.; Toney, M. F.; Salleo, A. The Chemical and Structural Origin of Efficient p-Type Doping in P3HT. *Org. Electron.* **2013**, *14*, 1330−1336.
(30) Pingel, P.; Neher, D. Comprehensive Picture of P-Type Doping of P3HT with the Molecular Acceptor F4TCNQ. *Phys. Rev. B: Condens. Matter Mater. Phys.* **2013**, *87*, 115209.
(31) Chiang, C. K.; Fincher, C. R.; Park, Y. W.; Heeger, A. J.; Shirakawa, H.; Louis, E. J.; Gau, S. C.; MacDiarmid, A. G. Electrical Conductivity in Doped Polyacetylene. *Phys. Rev. Lett.* **1977**, *39*, 1098−1101.
(32) Salzmann, I.; Heimel, G. Toward a Comprehensive Understanding of Molecular Doping Organic Semiconductors (Review). *J. Electron Spectrosc. Relat. Phenom.* **2015**, *204*, 208−222.
(33) Patel, S. N.; Glaudell, A. M.; Peterson, K. A.; Thomas, E. M.; O'Hara, K. A.; Lim, E.; Chabinyc, M. L. Morphology Controls the Thermoelectric Power Factor of a Doped Semiconducting Polymer. *Science Advances* **2017**, *3*, e1700434.
(34) Glaudell, A. M.; Cochran, J. E.; Patel, S. N.; Chabinyc, M. L. Impact of the Doping Method on Conductivity and Thermopower in Semiconducting Polythiophenes. *Adv. Energy Mater.* **2015**, *5*, 1401072.
(35) Jha, A.; Duan, H.-G.; Tiwari, V.; Thorwart, M.; Miller, R. J. D. Origin of Poor Doping Efficiency in Solution Processed Organic Semiconductors. *Chemical Science* **2018**, *9*, 4468.
(36) Gao, J.; Roehling, J. D.; Li, Y.; Guo, H.; Moule, A. J.; Grey, J. K. The Effect of 2,3,5,6-Tetrafluoro-7,7,8,8-tetracyanoquinodimethane Charge Transfer Dopants on the Conformation and Aggregation of Poly(3-hexylthiophene). *J. Mater. Chem. C* **2013**, *1*, 5638−5646.
(37) Gao, J.; Niles, E. T.; Grey, J. K. Aggregates Promote Efficient Charge Transfer Doping of Poly(3-hexylthiophene). *J. Phys. Chem. Lett.* **2013**, *4*, 2953−2957.
(38) Deschler, F.; Riedel, D.; Deák, A.; Ecker, B.; von Hauff, E.; Da Como, E. Imaging of Morphological Changes and Phase Segregation in Doped Polymeric Semiconductors. *Synth. Met.* **2015**, *199*, 381−387.
(39) Müller, L.; Nanova, D.; Glaser, T.; Beck, S.; Pucci, A.; Kast, A. K.; Schröder, R. R.; Mankel, E.; Pingel, P.; Neher, D.; et al. Charge-Transfer-Solvent Interaction Predefines Doping Efficiency in p-Doped P3HT Films. *Chem. Mater.* **2016**, *28*, 4432−4439.
(40) Kang, K.; Watanabe, S.; Broch, K.; Sepe, A.; Brown, A.; Nasrallah, I.; Nikolka, M.; Fei, Z.; Heeney, M.; Matsumoto, D.; et al. 2D Coherent Charge Transport in Highly Ordered Conducting Polymers Doped by Solid State Diffusion. *Nat. Mater.* **2016**, *15*, 896−903.
(41) Hynynen, J.; Kiefer, D.; Yu, L.; Kroon, R.; Munir, R.; Amassian, A.; Kemerink, M.; Müller, C. Enhanced Electrical Conductivity of Molecularly p-Doped Poly(3-hexylthiophene) Through Understand-

DOI: 10.1021/acs.jpcc.9b05069
J. Phys. Chem. C 2019, 123, 22711−22724

ing the Correlation with Solid-State Order. *Macromolecules* **2017**, *50*, 8140−8148.
(42) Lim, E.; Peterson, K. A.; Su, G. M.; Chabinyc, M. L. Thermoelectric Properties of Poly(3-hexylthiophene) (P3HT) Doped with 2,3,5,6-Tetrafluoro-7,7,8,8-tetracyanoquinodimethane (F4TCNQ) by Vapor-Phase Infiltration. *Chem. Mater.* **2018**, *30*, 998−1010.
(43) Hynynen, J.; Kiefer, D.; Müller, C. Influence of crystallinity on the Thermoelectric Power Factor of P3HT Vapour-Doped with F4TCNQ. *RSC Adv.* **2018**, *8*, 1593−1599.
(44) Jacobs, I. E.; Aasen, E. W.; Oliveira, J. L.; Fonseca, T. N.; Roehling, J. D.; Li, J.; Zhang, G.; Augustine, M. P.; Mascal, M.; Moulé, A. J. Comparison of Solution-Mixed and Sequentially Processed P3HT:F4TCNQ Films: Effect of Doping-Induced Aggregation on Film Morphology. *J. Mater. Chem. C* **2016**, *4*, 3454−3466.
(45) Zuo, G.; Andersson, O.; Abdalla, H.; Kemerink, M. High Thermoelectric Power Factor from Multilayer Solution-Processed Organic Films. *Appl. Phys. Lett.* **2018**, *112*, 083303.
(46) Patel, S. N.; Glaudell, A. M.; Kiefer, D.; Chabinyc, M. L. Increasing the Thermoelectric Power Factor of a Semiconducting Polymer by Doping from the Vapor Phase. *ACS Macro Lett.* **2016**, *5*, 268−272.
(47) Xuan, Y.; Liu, X.; Desbief, S.; Leclère, P.; Fahlman, M.; Lazzaroni, R.; Berggren, M.; Cornil, J.; Emin, D.; Crispin, X. Thermoelectric Properties of Conducting Polymers: The case of Poly(3-hexylthiophene). *Phys. Rev. B: Condens. Matter Mater. Phys.* **2010**, *82*, 115454.
(48) Gregory, S. A.; Menon, A. K.; Ye, S.; Seferos, D. S.; Reynolds, J. R.; Yee, S. K. Effect of Heteroatom and Doping on the Thermoelectric Properties of Poly (3-alkylchalcogenophenes). *Adv. Energy Mater.* **2018**, *8*, 1802419.
(49) Hawks, S. A.; Aguirre, J. C.; Schelhas, L. T.; Thompson, R. J.; Huber, R. C.; Ferreira, A. S.; Zhang, G.; Herzing, A. A.; Tolbert, S. H.; Schwartz, B. J. Comparing Matched Polymer:Fullerene Solar Cells Made by Solution-Sequential Processing and Traditional Blend Casting: Nanoscale Structure and Device Performance. *J. Phys. Chem. C* **2014**, *118*, 17413−17425.
(50) Aguirre, J. C.; Hawks, S. A.; Ferreira, A. S.; Yee, P.; Subramaniyan, S.; Jenekhe, S. A.; Tolbert, S. H.; Schwartz, B. J. Sequential Processing for Organic Photovoltaics: Design Rules for Morphology Control by Tailored Semi-Orthogonal Solvent Blends. *Adv. Energy Mater.* **2015**, *5*, 1402020.
(51) Fontana, M. T.; Kang, H.; Yee, P. Y.; Fan, Z.; Hawks, S. A.; Schelhas, L. T.; Subramaniyan, S.; Hwang, Y. J.; Jenekhe, S. A.; Tolbert, S. H.; et al. Low-Vapor-Pressure Solvent Additives Function as Polymer Swelling Agents in Bulk Heterojunction Organic Photovoltaics. *J. Phys. Chem. C* **2018**, *122*, 16574−16588.
(52) Li, J.; Zhang, G.; Holm, D. M.; Jacobs, I. E.; Yin, B.; Stroeve, P.; Mascal, M.; Moulé, A. J. Introducing Solubility Control for Improved Organic P-Type Dopants. *Chem. Mater.* **2015**, *27*, 5765−5774.
(53) Ayzner, A. L.; Tassone, C. J.; Tolbert, S. H.; Schwartz, B. J. Reappraising the Need for Bulk Heterojunctions in Polymer-Fullerene Photovoltaics: The Role of Carrier Transport in All-Solution-Processed P3HT/PCBM Bilayer Solar Cells. *J. Phys. Chem. C* **2009**, *113*, 20050−20060.
(54) Aguirre, J. C.; Ferreira, A.; Ding, H.; Jenekhe, S. A.; Kopidakis, N.; Asta, M.; Pilon, L.; Rubin, Y.; Tolbert, S. H.; Schwartz, B. J.; et al. Panoramic View of Electrochemical Pseudocapacitor and Organic Solar Cell Research in Molecularly Engineered Energy Materials. *J. Phys. Chem. C* **2014**, *118*, 19505−19523.
(55) Aubry, T. J.; Axtell, J. C.; Basile, V. M.; Winchell, K. J.; Lindemuth, J. R.; Porter, T. M.; Liu, J. Y.; Alexandrova, A. N.; Kubiak, C. P.; Tolbert, S. H.; et al. Dodecaborane-Based Dopants Designed to Shield Anion Electrostatics Lead to Increased Carrier Mobility in a Doped Conjugated Polymer. *Adv. Mater.* **2019**, *31*, 1805647.
(56) Che, C.-M.; Roy, V. A. L.; Xiang, H.-F.; Lai, P. T.; Xu, Z.-X. Method for Measurement of the Density of Thin Films of Small Organic Molecules. *Rev. Sci. Instrum.* **2007**, *78*, 034104.
(57) NIST *Resistivity and Hall Measurements*. 2018; https://www.nist.gov/pml/engineering-physics-division/popular-links/hall-effect/resistivity-and-hall-measurements#resistivity.
(58) Hynynen, J.; Järsvall, E.; Kroon, R.; Zhang, Y.; Barlow, S.; Marder, S. R.; Kemerink, M.; Lund, A.; Müller, C. Enhanced Thermoelectric Power Factor of Tensile Drawn Poly(3-hexylthiophene). *ACS Macro Lett.* **2019**, *8*, 70−76.
(59) Reiser, P.; Müller, L.; Sivanesan, V.; Lovrincic, R.; Barlow, S.; Marder, S. R.; Pucci, A.; Jaegermann, W.; Mankel, E.; Beck, S. Dopant Diffusion in Sequentially Doped Poly(3-hexylthiophene) Studied by Infrared and Photoelectron Spectroscopy. *J. Phys. Chem. C* **2018**, *122*, 14518−14527.
(60) Li, J.; Koshnick, C.; Diallo, S. O.; Ackling, S.; Huang, D. M.; Jacobs, I. E.; Harrelson, T. F.; Hong, K.; Zhang, G.; Beckett, J.; et al. Quantitative Measurements of the Temperature-Dependent Microscopic and Macroscopic Dynamics of a Molecular Dopant in a Conjugated Polymer. *Macromolecules* **2017**, *50*, 5476−5489.
(61) Hase, H.; O'Neill, K.; Frisch, J.; Opitz, A.; Koch, N.; Salzmann, I. Unraveling the Microstructure of Molecularly Doped Poly(3-hexylthiophene) by Thermally Induced Dedoping. *J. Phys. Chem. C* **2018**, *122*, 25893−25899.
(62) Wang, C.; Duong, D. T.; Vandewal, K.; Rivnay, J.; Salleo, A. Optical Measurement of Doping Efficiency in Poly(3-hexylthiophene) Solutions and Thin Films. *Phys. Rev. B: Condens. Matter Mater. Phys.* **2015**, *91*, 085205.
(63) Chew, A. R.; Ghosh, R.; Shang, Z.; Spano, F. C.; Salleo, A. Sequential Doping Reveals the Importance of Amorphous Chain Rigidity in Charge Transport of Semi-Crystalline Polymers. *J. Phys. Chem. Lett.* **2017**, *8*, 4974−4980.
(64) Voss, M. G.; Scholes, D. T.; Challa, J. R.; Schwartz, B. J. Ultrafast Transient Absorption Spectroscopy of Doped P3HT Films: Distinguishing Free and Trapped Polarons. *Faraday Discuss.* **2019**, *216*, 339−362.
(65) Karpov, Y.; Kiriy, N.; Al-Hussein, M.; Hambsch, M.; Beryozkina, T.; Bakulev, V.; Mannsfeld, S. C.; Voit, B.; Kiriy, A. Hexacyano-[3]-Radialene Anion-Radical Salts: A Promising Family of Highly Soluble p-Dopants. *Chem. Commun.* **2018**, *54*, 307−310.
(66) Beiley, Z. M.; Hoke, E. T.; Noriega, R.; Dacuña, J.; Burkhard, G. F.; Bartelt, J. A.; Salleo, A.; Toney, M. F.; McGehee, M. D. Morphology-Dependent Trap Formation in High Performance Polymer Bulk Heterojunction Solar Cells. *Adv. Energy Mater.* **2011**, *1*, 954−962.
(67) Liu, Y.; Zhao, J.; Li, Z.; Mu, C.; Ma, W.; Hu, H.; Jiang, K.; Lin, H.; Ade, H.; Yan, H. Aggregation and Morphology Control Enables Multiple Cases of High-Efficiency Polymer Solar Cells. *Nat. Commun.* **2014**, *5*, 5293.
(68) Verploegen, E.; Mondal, R.; Bettinger, C. J.; Sok, S.; Toney, M. F.; Bao, Z. Effects of Thermal Annealing Upon the Morphology of Polymer-Fullerene Blends. *Adv. Funct. Mater.* **2010**, *20*, 3519−3529.
(69) Zhokhavets, U.; Erb, T.; Hoppe, H.; Gobsch, G.; Serdar Sariciftci, N. Effect of Annealing of Poly(3-hexylthiophene)/Fullerene Bulk Heterojunction Composites on Structural and Optical Properties. *Thin Solid Films* **2006**, *496*, 679−682.
(70) Salleo, A.; Kline, R. J.; DeLongchamp, D. M.; Chabinyc, M. L. Microstructural Characterization and Charge Transport in Thin Films of Conjugated Polymers. *Adv. Mater.* **2010**, *22*, 3812−3838.
(71) Wohlgenannt, M.; Jiang, X. M.; Vardeny, Z. V. Confined and Delocalized Polarons in π-conjugated Oligomers and Polymers: A Study of the Effective Conjugation Length. *Phys. Rev. B: Condens. Matter Mater. Phys.* **2004**, *69*, 241204.
(72) Pochas, C. M.; Spano, F. C. New Insights on the Nature of Two-Dimensional Polarons in Semiconducting Polymers: Infrared Absorption in Poly(3-hexylthiophene). *J. Chem. Phys.* **2014**, *140*, 244902.
(73) Ghosh, R.; Pochas, C. M.; Spano, F. C. Polaron Delocalization in Conjugated Polymer Films. *J. Phys. Chem. C* **2016**, *120*, 11394−11406.
(74) Ghosh, R.; Chew, A. R.; Onorato, J.; Pakhnyuk, V.; Luscombe, C. K.; Salleo, A.; Spano, F. C. Spectral Signatures and Spatial

DOI: 10.1021/acs.jpcc.9b05069
J. Phys. Chem. C 2019, 123, 22711−22724

Coherence of Bound and Unbound Polarons in P3HT Films: Theory Versus Experiment. *J. Phys. Chem. C* **2018**, *122*, 18048−18060.

DOI: 10.1021/acs.jpcc.9b05069
J. Phys. Chem. C 2019, 123, 22711−22724